Glucose and glutamine fuel protein O-GlcNAcylation to control T cell self-renewal and malignancy

Mahima Swamy[1], **Shalini Pathak**[1], **Katarzyna M. Grzes**[1], **Sebastian Damerow**[2], **Linda V. Sinclair**[1], **Daan M. F. van Aalten**[3], and **Doreen A. Cantrell**[1]

[1]Division of Cell Signalling and Immunology, University of Dundee, United Kingdom

[2]Division of Biological Chemistry and Drug Discovery, University of Dundee, United Kingdom

[3]Medical Research Council Protein Phosphorylation and Ubiquitylation unit, University of Dundee, United Kingdom

Abstract

Sustained glucose and glutamine transport are essential for activated T lymphocytes to support ATP and macromolecule biosynthesis. We now show that glutamine and glucose also fuel an indispensible dynamic regulation of intracellular protein O-GlcNAcylation at key stages of T cell development, transformation and differentiation. Glucose and glutamine are precursors of UDP-GlcNAc, a substrate for cellular glycosyltransferases. Immune activated T cells contained higher concentrations of UDP-GlcNAc and increased intracellular protein O-GlcNAcylation controlled by the enzyme O-GlcNAc glycosyltransferase as compared to naïve cells. We identified Notch, the T cell antigen receptor and c-Myc as key controllers of T cell protein O-GlcNAcylation, via regulation of glucose and glutamine transport. Loss of O-GlcNAc transferase blocked T cell progenitor renewal, malignant transformation, and peripheral T cell clonal expansion. Nutrient-dependent signaling pathways regulated by O-GlcNAc glycosyltransferase are thus fundamental for T cell biology.

One function of antigen and cytokine controlled signaling pathways in T cells is to regulate expression of nutrient transporters and metabolic enzymes to meet the metabolic demands during thymus development and immune responses1. Increased capacity to transport glucose and amino acids is essential to fuel oxidative phosphorylation, glycolysis, and *de novo* protein synthesis in activated T cells. The supply of glucose, leucine and glutamine in T cells also controls the activity of mammalian Target of Rapamycin Complex 1 (mTORC1)2–4. Additionally, glutamine can be directed into glutaminolysis to produce key metabolic

intermediates pyruvate and lactate, precursors for fatty acid biosynthesis and ATP production from the citric acid cycle1,5.

One other metabolic route for glucose and glutamine is the hexosamine biosynthetic pathway (HBP), which controls the production of UDP-GlcNAc (uridine diphosphate N-acetylglucosamine). UDP-GlcNAc is metabolized by glycosyltransferases to produce glycoproteins, proteoglycans and glycolipids. It is also the donor substrate for O-GlcNAc transferase (OGT), a unique enzyme that catalyzes the addition of O-linked-β-N-acetylglucosamine (O-GlcNAc) to serine or threonine residues on intracellular proteins6. This post-translational modification is reversible and the cleavage of O-GlcNAc from modified proteins is controlled by a single glycoside hydrolase known as O-GlcNAcase (OGA)6. O-GlcNAcylation can compete with phosphorylation for modification of serine or threonine residues allowing dynamic crosstalk between these modifications, that can change the output of Ser/Thr kinase-mediated signaling pathways7–9. O-GlcNAcylation is an essential process that can also directly control protein stability, localization, transcriptional activity and multiple other cellular functions6,10. OGT is moreover indispensible for murine embryo development and for thymus development11,12.

Precise regulation of glucose and glutamine transport is essential for T cells4,13. It has also been described that ConA activation of T cells causes transient increase of intracellular protein O-GlcNAcylation14 and c-Rel and NFAT have been reported to be OGT substrates in T cells15,16. However, there is little information about the regulation of the HBP or protein O-GlcNAcylation in T cells, or about the dynamics of O-GlcNAcylation in peripheral T cells. In the present study, we show that at key stages of T cell development and activation, as well as in malignant T cells, glucose and glutamine are directed through the HBP to support dynamic intracellular protein O-GlcNAcylation. We show that Notch, the T cell antigen receptor (TCR), and the transcription factor c-Myc regulate protein O-GlcNAcylation at different stages of T cell development and activation. We also show that OGT is critical for Notch-mediated self-renewal of T cell progenitors in the thymus; for T cell malignant transformation; and for the clonal expansion of TCR-activated peripheral T cells. Hence the modification of proteins such as c-Myc by O-GlcNAcylation links nutrient transport to the control of T cell function: a previously unappreciated but essential role of glucose and glutamine metabolism in T cells.

Results

Increased UDP-GlcNAc synthesis in TCR-triggered T cells

Triggering of the TCR on naïve T lymphocytes increases expression of glucose and glutamine transporters5 and glucose and glutamine transport (Fig. 1a)4,17–19. TCR-primed $CD8^+$ T cells cultured in interleukin 2 (IL-2) clonally expand and differentiate to cytotoxic T cells (CTLs) that have very high rates of glucose and glutamine transport (Fig. 1b). Similarly, there was increased glucose and glutamine transport in 'T_H1' $CD4^+$ effector cells (Fig. 1b). Glucose and glutamine can be metabolized via the HBP to make UDP-GlcNAc (Fig. 1c). We therefore used liquid chromatography-electrospray ionization-tandem mass spectrometry (LC-ES-MS/MS) to quantify UDP-GlcNAc content in T lymphocytes20 to explore whether immune activation modulates their intracellular UDP-GlcNAc pools. These

experiments revealed that TCR triggering of CD8$^+$ T cells with cognate peptide induced a striking increase in cellular UDP-GlcNAc concentrations (Fig. 1d). Moreover in effector CTLs, concentrations of UDP-GlcNAc were ~ 7×10^8 molecules per cell, a log increase compared to UDP-GlcNAc amounts in naïve T cells. There was also a significant increase in UDP-GlcNAc concentrations in activated CD4$^+$ T cells, with a 10-fold increase over naïve cells just 24 hours after TCR triggering (Fig. 1e). Effector CD4$^+$ T cells had ~ 3×10^8 UDP-GlcNAc molecules per cell, about half as much as CTLs, which correlated with the lower glucose and glutamine uptake measured in T$_H$1 CD4$^+$ effectors as compared to CTLs (Fig. 1b). The production of UDP-GlcNAc was necessarily dependent on external glucose and glutamine supply (Fig. 1f). Importantly, the supply of glucosamine could vastly increase UDP-GlcNAc concentrations in nutrient-starved T cells, consistent with the model that T cells control cellular levels of UDP-GlcNAc via the HBP, and that nutrient uptake and conversion to glucosamine-6-phosphate are rate-limiting in T cells (Fig.1c,g).

Dynamic regulation of O-GlcNAcylation in T cells

UDP-GlcNAc is a substrate for OGT, the enzyme that controls the modification of intracellular proteins by O-GlcNAc. We considered the possibility that changes in the availability of UDP-GlcNAc might promote changes in protein O-GlcNAcylation in immune activated T cells. Immunoblot analysis with an O-GlcNAc specific antibody (RL2) revealed a strong increase in O-GlcNAcylation of multiple proteins in antigen receptor activated CD8$^+$ T cells compared to naïve T cells (Fig. 2a). Effector CTLs also had high levels of protein O-GlcNAcylation (Fig. 2b). Pre-treatment of the CTLs lysates with the bacterial O-GlcNAcase, CpOGA21, or antibody competition with N-Acetylglucosamine (GlcNAc), confirmed the specificity of the antibody for O-GlcNAcylated proteins (Fig. 2b). To quantitatively monitor protein O-GlcNAcylation during T cell activation we developed an intracellular flow cytometric assay with the RL2 antibody. Activated CTLs exhibited higher RL2 intracellular staining as compared to naïve T cells (Fig. 2c) and this staining was effectively competed by the free GlcNAc sugar (Fig. 2d). Treating permeabilized CTLs with CpOGA, which removes O-GlcNAc from proteins, reduced RL2 staining (Fig. 2e). There was no strong correlation between RL2 staining intensity and cell size (Fig. 2f). Importantly, there was no RL2 staining in non-permeabilized activated T cells (Fig. 2g) confirming that these RL2 analyses detect intracellular protein O-GlcNAcylation, and not surface protein glycosylation.

Using this assay, we saw a rapid and sustained increase in RL2 staining in CD4$^+$ and CD8$^+$ T cells activated with CD3 and CD28 antibodies (Fig. 2h). There were also increases in RL2 staining in OT-I TCR transgenic T cells triggered with their cognate peptide (Fig. 2i). TCR activation is regulated by the quantity and affinity of the TCR ligand and the increase in intracellular protein O-GlcNAcylation in TCR-activated OT-I cells was commensurate with the quality and quantity of the TCR ligand (Fig. 2i,,j). We also found that activated T cells from mice infected with *Listeria monocytogenes* had enhanced protein O-GlcNAcylation as compared to non-activated T cells from the same mice (Fig. 2k,l). Thus *in vitro* and *in vivo*, T cells actively regulate intracellular protein O-GlcNAcylation. The increases in protein O-GlcNAcylation are relatively rapid responses (within 6 hours) to T cell activation and precede the increases in cell size and cell cycle progression that accompany T cell activation.

To assess whether protein O-GlcNAcylation was dynamically regulated in T cells, CTLs were treated with a metabolic OGT inhibitor (4AC-5S-GlcNAc22) or with an OGA inhibitor (GlcNAcstatin G23). Within 30 minutes of treatment with either inhibitor, changes in the O-GlcNAc levels in the CTLs were apparent. O-GlcNAc levels decreased in cells treated with the OGT inhibitor, and O-GlcNAc levels increased in CTLs treated with the OGA inhibitor (Fig. 2m). Intriguingly, inhibition of OGA lead to a maximal increase in O-GlcNAc levels of ~1.5-fold, even with longer incubation times (Fig. 2m), whereas OGT inhibition lead to a near complete loss of O-GlcNAc staining within 24 hours. These data suggest that CTLs have close to saturating amounts of protein O-GlcNAcylation and reveal the dynamic nature of protein O-GlcNAcylation in T cells.

Protein O-GlcNAcylation during thymocyte β-selection

Having established that O-GlcNAc levels increased following TCR activation of peripheral T cells, we next explored the link between metabolism and intracellular protein O-GlcNAcylation during thymocyte development. In particular, we wished to investigate whether the increased glucose metabolism that is controlled by Notch signaling in T cell progenitors24 was associated with changes in protein O-GlcNAcylation. T cell progenitors that lack expression of the MHC co-receptors CD4 and CD8 (double-negative (DN) thymocytes) initiate rearrangements of their *Tcrb* locus and if successful, produce a TCRβ chain that permits pre-TCR complex expression. This stage of T cell development occurs in DN3 thymocytes (CD4$^-$CD8$^-$CD44$^-$CD25$^+$). The pre-TCR, in combination with Notch and IL-7, promotes the proliferation and differentiation of DN3s into the DN4 stage of pre-T cell development (CD4$^-$CD8$^-$CD44$^-$CD25$^-$), a process known as β-selection25,26. β-selected DN4 cells then undergo rapid self-renewal and differentiate into CD4$^+$CD8$^+$double-positive (DP) thymocytes. The rapid proliferation of β-selected DN4s is fueled by regulated changes in the metabolism of these cells27. Indeed, DN3 thymocytes have low rates of glucose and glutamine uptake whereas β-selected DN4 thymocytes upregulate both glucose and glutamine transport; DPs return to a state of very low levels of glucose and glutamine uptake (Fig. 3a). Interestingly, there was a concomitant dynamic regulation of protein O-GlcNAcylation during these stages of thymocyte development (Fig. 3b). Protein O-GlcNAcylation was upregulated as DN3 thymocytes differentiated to β-selected DN4 thymocytes. The further differentiation of β-selected cells to DPs was accompanied by a striking reduction of protein O-GlcNAcylation (Fig. 3b).

The metabolic changes that support the DN-to-DP stage of thymocyte differentiation are controlled by Notch24,28. We therefore wanted to address the role of Notch ligands in regulating protein O-GlcNAcylation in thymocytes. Hence, we used the OP9-DL1 system of *in vitro* thymocyte differentiation29 where OP9 cells expressing the Notch ligand delta-like 1 (DL1) support the differentiation and self-renewal of β-selected DN3 thymocytes. This *in vitro* model recapitulates the *in vivo* scenario where Notch drives the rapid proliferation/self-renewal of TCRβ expressing DN4s and supports their differentiation to DPs25,30,31. DN thymocytes maintained in IL-7 on either OP9 or OP9-DL1 cells had low rates of glucose and glutamine transport which contrasted with the high rates of glucose and glutamine uptake in Notch-stimulated cells (Fig. 3c). In parallel with changes in glucose and glutamine transport, DN thymocytes stimulated with Notch ligands increased intracellular protein O-

GlcNAcylation (Fig. 3d). Similar to the *in vivo* data, as thymocytes differentiated to DPs on OP9-DL1, they reverted to low intracellular O-GlcNAcylation (Fig. 3e). Thus, trophic Notch signals control OGT mediated protein O-GlcNAcylation in T cell progenitors in the thymus.

O-GlcNAcylation in Notch-induced pre-T cell self-renewal

Analysis of protein O-GlcNAcylation during T cell development indicated that this modification was tightly regulated by metabolic changes during the DN3-DN4 stages. To explore the importance of protein O-GlcNAcylation in pre-T cells, we generated $Ogt^{fl/fl}Lck$-Cre mice. *Lck*-Cre expression permits deletion of OGT in the DN progenitor stage of thymocyte development. Thymocyte numbers in $Ogt^{fl/fl}Lck$-Cre$^+$ mice were reduced by 70% (Fig. 4a), due to the drastic reduction of DPs and positively selected CD4-SP or CD8-SP thymocytes caused by OGT loss (Fig. 4b,c). $Ogt^{fl/fl}Lck$-Cre$^+$ mice also had a striking reduction in mature T cells in the periphery indicative of failed thymocyte development (Supplementary Fig. 1a). Intracellular staining with the RL2 antibody confirmed loss of protein O-GlcNAcylation in DN4 and DP thymocytes from $Ogt^{fl/fl}Lck$-Cre$^+$ mice (Fig. 4d).

The phenotype of $Ogt^{fl/fl}Lck$-Cre$^+$ thymi was consistent with a failure of β-selection. However, DN4 cells from $Ogt^{fl/fl}Lck$-Cre$^+$ mice expressed normal levels of intracellular TCRβ subunits indicating that they had successfully rearranged their *Tcrb* locus (Fig. 4e). Thymocyte subsets from $Ogt^{fl/fl}Lck$-Cre$^+$ mice also expressed normal levels of Notch1, Notch2 and IL-7R (Supplementary Fig. 1b), and there were comparable DN4 thymocyte numbers in $Ogt^{fl/fl}Lck$-Cre$^+$ mice and wild-type mice (Supplementary Fig. 1c). The failure to produce normal numbers of DPs from TCR -expressing DN4s could reflect a failure of differentiation or a failure of clonal expansion. It has also been proposed that loss of OGT might cause increased apoptosis of DP thymocytes12. To distinguish these possibilities we examined the ability of DN thymocytes from $Ogt^{fl/fl}Lck$-Cre$^+$ mice to differentiate and proliferate on OP9-DL1 feeder cells. DN cells from $Ogt^{fl/fl}Lck$-Cre$^+$ mice were able to differentiate to DPs when cultured on OP9-DL1 or OP9 cells (Fig. 4f,g). Moreover, OGT-null DN thymocytes survived normally when cultured in the presence of IL-7 on the OP9 feeder cells lacking DL1 (Fig. 4h). However, in contrast to wild-type DNs, they failed to proliferate in response to IL-7 and DL1 (Fig. 4i). The loss of OGT thus did not prevent T cell progenitors from surviving or differentiating to the DP stage of thymocyte development. Rather, OGT was required for the rapid self-renewal of TCR β-selected cell progenitors.

Malignant transformation of T cell progenitors needs OGT

T cell progenitors can undergo transformation to produce T cell leukemia/lymphoma upon deletion of tumor suppressors or oncogene expression32,33. Transformed cells are known to have high rates of glucose transport. We therefore wanted to explore the protein O-GlcNAcylation characteristics of transformed T cell progenitors. $Pten^{fl/fl}Lck$-Cre$^+$ mice serve as a murine model for T-cell acute lymphoblastic leukemia (T-ALL)34,35. *Pten* deletion in T cell progenitors in $Pten^{fl/fl}Lck$-Cre$^+$ mice results in the development of aggressive, fatal T cell lymphomas in the thymus around 8-12 weeks after birth33,35. These transformed cells are dependent on Notch1- or c-Myc-induced signals27. T lymphoma cells isolated from $Pten^{fl/fl}Lck$-Cre$^+$ mice had very high levels of glucose and glutamine uptake compared to non-transformed thymocytes (Fig. 5a,b). These high levels of glucose and

glutamine uptake translated to high levels of O-GlcNAcylation in the transformed cells compared to wild-type thymocytes (Fig. 5c). We assessed the importance of intracellular protein O-GlcNAcylation for T cell malignancy by backcrossing the $Pten^{fl/fl}Lck$-Cre mice with $Ogt^{fl/fl}$ mice to generate mice that lacked both PTEN and OGT in T cell progenitors ($Pten^{fl/fl}Ogt^{fl/fl}Lck$-Cre). As described35, $Pten^{fl/fl}Lck$-Cre$^+$ mice had a median survival age of ~12-13 weeks (Fig. 5d). There was however a striking difference in survival of $Pten^{fl/fl}Lck$-Cre$^+$ mice versus $Pten^{fl/fl}Ogt^{fl/fl}Lck$-Cre$^+$ (DKO) mice. Remarkably, deletion of Ogt completely rescued mice from PTEN-deficiency induced morbidities, and all mice (n=10) survived >30 weeks, at which point they were culled for analysis (Fig. 5d). Thymocyte numbers were still vastly lower in DKO versus wild-type mice (Fig. 5e) and the cells were unable to differentiate into CD4SP or CD8SP (Fig. 5f). The deletion of $Pten$ could thus not overcome the thymus developmental block caused by OGT loss. Moreover, $Pten$ deletion could not induce the malignant transformation of OGT-null T cell progenitors, despite the DKO mice having normal numbers of pre-T cells.

Dynamic O-GlcNAcylation in thymocyte positive selection

The purpose of the rapid self-renewal of β-selected DN4 thymocytes is to create a pool of DP thymocytes that can then rearrange their $Tcra$ locus. If rearrangements are successful, a functional TCRαβ complex is expressed on DPs that can recognize self-antigen-MHC complexes. DP thymocytes can then be activated by TCR-mediated signals to differentiate to CD4SP or CD8SP cells (positive selection). TCR triggering of peripheral T cells increases intracellular protein O-GlcNAcylation. Therefore we asked whether protein O-GlcNAcylation was also regulated during thymocyte positive selection. TCRβ^{hi}CD69$^+$cells define positively selecting DPs and TCRβ^{hi}CD69^{lo}CD24^{lo} cells define mature SP cells that are ready to exit the thymus to populate the periphery. We found that O-GlcNAc levels increased as DP thymocytes respond to TCR-driven positive selection signals and upregulated CD69 and TCR expression (Fig. 6a). Moreover, as the cells differentiated to mature CD4SP or CD8SP thymocytes they upregulated their protein O-GlcNAcylation levels even further (Fig. 6a).

To explore the functional significance of the increase in protein O-GlcNAcylation that accompanied the differentiation of DP thymocytes to CD4SP and CD8SP cells, we generated $Ogt^{fl/fl}Cd4$-Cre$^+$ mice. $Cd4$-Cre deletes just before the DP stage in the thymus. We found normal numbers of DP thymocytes in $Ogt^{fl/fl}Cd4$-Cre$^+$ mice (Fig. 6b, Supplementary Fig. 2b). However, $Ogt^{fl/fl}Cd4$-Cre$^+$ mice failed to produce SP thymocytes or mature T cells (Fig. 6b-d, Supplementary Fig. 2c). We confirmed that the DP thymocytes that were present in normal numbers in $Ogt^{fl/fl}Cd4$-Cre$^+$ mice had lost OGT (Fig. 6e), indicating that OGT was not necessary for DP survival. Moreover, these cells were able to initiate positive selection and upregulate CD69, a marker of successful engagement of the αβTCR with positively selecting TCR ligands (Fig. 6f). However, the OGT-null DP thymocytes could not complete positive selection and differentiate to TCRβ^{hi} mature SP thymocytes (Fig. 6f). Thus protein O-GlcNAcylation is both dynamic and essential during thymocyte positive selection.

The role of OGT in mature T cell clonal expansion

No mature T cells were generated in either $Ogt^{fl/fl}Lck$-Cre$^+$ or $Ogt^{fl/fl}Cd4$-Cre$^+$ mice. Therefore, to address the role of OGT in T cell function, we generated an inducible mouse model for OGT deletion. We backcrossed $Ogt^{fl/fl}$ mice with Tamox-Cre mice that constitutively express a hydroxytamoxifen-regulated Cre recombinase. This model permits rapid deletion of floxed alleles following treatment of cells with 4-hydroxytamoxifen (4-OHT). 4-OHT mediated deletion of OGT in naïve T cells from $Ogt^{fl/fl}$Tamox-Cre$^+$ mice prevented antigen receptor-induced proliferative expansion (Fig. 7a). We also generated CTLs from $Ogt^{fl/fl}$Tamox-Cre$^+$ mice and treated these cells with 4-OHT to delete the floxed OGT alleles directly in effector CTLs. The loss of OGT and protein O-GlcNAcylation was confirmed by immunoblotting (Supplementary Fig. 3). Clonal expansion of CTLs is controlled by the cytokine IL-2. OGT-null CTLs survived in IL-2 but failed to proliferate (Fig. 7b). IL-2 controls CTLs via signaling pathways mediated by STAT5, mTORC1 and c-Myc[19,36,37]. The loss of OGT did not impair IL-2-induced phosphorylation of STAT5 or IL-2-driven mTORC1 activity (Fig. 7c). In contrast, loss of OGT in CTLs resulted in loss of c-Myc expression (Fig. 7c). To further explore the correlation between protein O-GlcNAcylation and c-Myc expression in T cells we used a *GFP-c-Myc* knockin mouse model (*GFP-Myc*^{KI})[38] to examine the impact of OGT and OGA inhibitors on c-Myc expression. TCR-activated T cells expressed high levels of c-Myc[37], but c-Myc expression levels were much lower when T cells were activated in the presence of an OGT inhibitor (Fig. 7d). Conversely, when T cells were activated in the presence of an OGA inhibitor, c-Myc expression increased (Fig. 7d). c-Myc expression in T cells is regulated post-translationally by GSK3-mediated phosphorylation of c-Myc Thr58, a modification that targets c-Myc for proteolytic degradation[37]. However, c-Myc can also be O-GlcNAcylated on Thr58 (ref. 39), which would prevent phosphorylation on this site and stabilize c-Myc protein. The sensitivity of Myc expression to OGT/OGA activity is consistent with c-Myc O-GlcNAcylation playing a role in controlling c-Myc expression in T cells. Indeed c-Myc could be affinity purified from CTLs lysates with succinylated wheat germ agglutinin (sWGA) which selectively binds to GlcNAcylated proteins (Fig. 7e). Moreover, the RL2 antibody could detect GFP-Myc immune-purified from CTLs lysates, but this RL2 immuno-reactivity was lost when GFP-Myc was immune-purified from CTLs lysates pre-treated with CpOGA to remove O-GlcNAc (Fig. 7f). c-Myc is thus O-GlcNAcylated in T cells and its expression is regulated by OGT.

Glucose, glutamine supply regulate protein O-GlcNAcylation

High levels of protein O-GlcNAcylation were found in T cells with high levels of glucose and glutamine uptake that fuel the production of UDP-GlcNAc. However, the sensitivity of protein O-GlcNAcylation to nutrient supply in T cells has not been explored. When CTLs were cultured in medium with decreasing amounts of glucose or glutamine, protein O-GlcNAc levels were correspondingly reduced (Fig. 8a), and a similar pattern was seen in 6 hour activated T cells (Fig. 8b). TCR-induced increases in glucose and glutamine uptake are regulated by c-Myc, which controls expression of the key glucose and glutamine transporters[5]. We therefore explored the role of c-Myc in mediating TCR-induced changes in intracellular protein O-GlcNAcylation using T cells from $Myc^{fl/fl}Cd4$-Cre$^+$ mice that have T cell-selective deletion of c-Myc. In resting naïve T cells, levels of protein O-

GlcNAcylation were comparable between wild-type and $Myc^{fl/fl}Cd4$-Cre$^+$ mice. However only TCR-activated wild-type but not c-Myc-null T cells were able to upregulate protein O-GlcNAcylation (Fig. 8c).

We previously showed that adding glucosamine to glucose-deprived cells rescues UDP-GlcNAc. In immune-activated primary T cells we found that glucosamine could rescue the loss of protein O-GlcNAcylation induced by lack of glucose or glutamine (Fig. 8d). The expression of c-Myc, but not activation markers such as CD69, was similarly regulated by glucose and glutamine supply (Fig. 8e,f). TCR-activated T cells could thus not sustain expression of c-Myc or the Myc-regulated transferrin receptor37 (CD71) in the absence of exogenous glucose and glutamine. Importantly, the direct supply of glucosamine, that directly fuels UDP-GlcNAc production could restore global protein O-GlcNAcylation, c-Myc and transferrin receptor expression in glucose and glutamine starved activated T cells (Fig. 8d-g). Collectively these data show that glucose and glutamine supply fuel protein O-GlcNAcylation in T cells via the HBP, which in turn regulates c-Myc expression levels in a feedback loop.

Discussion

The present study has shown that T cells exhibit dynamic regulation of intracellular protein O-GlcNAcylation at key stages of development in the thymus, following immune challenge by pathogen *in vivo*, and as a direct response to TCR engagement with cognate peptide. There are also striking changes in protein O-GlcNAcylation in malignant T lymphoma cells. These changes in protein O-GlcNAcylation are fueled by regulated changes in glucose and glutamine supply and are balanced by the cellular activities of OGT, and the glycosidase OGA. OGT was shown to be critical for Notch mediated self-renewal and malignant transformation of β-selected T cell progenitors during thymus development. OGT is also required for thymocyte positive selection and to initiate and sustain the clonal expansion of immune activated peripheral T cells. The present study thus affords the insight that glucose and glutamine flux through the HBP to generate UDP-GlcNAc, the substrate for OGT-mediated protein O-GlcNAcylation, is regulated by antigen receptor engagement. OGT-mediated protein O-GlcNAcylation is a critical process for T cell function.

It is increasingly recognized that T cell metabolism may be compromised during chronic viral infections and in T cells within tumors, thus contributing to a state of T cell 'exhaustion' that prevents T cells exerting their effector function40–42. This may be particularly problematic when T cells are in microenvironments that are hypoxic40 or where there is strong competition for nutrients such as glucose41,42. So far the glucose requirements of activated T cells have been studied primarily in the context of glucose as a fuel for oxidative phosphorylation and glycolysis and as a building block for nucleotide and amino acid biosynthesis, while glutamine metabolism studies have mainly focused on protein synthesis and glutaminolysis. The present study shows that glucose and glutamine availability also dictates the crucial process of protein O-GlcNAcylation. OGT thus functions to integrate changes in glucose and glutamine supply to modify T cell biology. OGT acts as a master regulator that depends on nutrient levels to control the commitment of T cells to metabolically demanding processes of clonal expansion, self-renewal and

differentiation. OGT acts in the thymus as a checkpoint for Notch mediated control of T cell progenitors. It also acts as a checkpoint for TCR-mediated positive selection and for TCR-induced clonal expansion of peripheral T cells.

One experimental observation that would explain some of the phenotypes of OGT-null cells was the impact of OGT deletion on the expression of c-Myc. This proto-oncogene has a key role to control metabolism of thymocytes and peripheral T cells5. In the absence of c-Myc, triggering of the TCR in peripheral T cells is unable to sustain increases in protein O-GlcNAcylation. Conversely we noted that OGT inhibition or deletion was associated with a failure of activated T cells to sustain expression of c-Myc. In this context we show that c-Myc is O-GlcNAcylated in T cells and that its expression is regulated by glucose availability. This ability of c-Myc to function as a glucose sensor in T cells reflects that glucose fuels protein O-GlcNAcylation, and O-GlcNAcylation of c-Myc promotes c-Myc stabilization. Collectively the present study reveals an essential positive feedback loop linking OGT-mediated pathways of protein O-GlcNAcylation in T cells to c-Myc expression. The failure to sustain c-Myc expression would explain the failure of OGT null T cell progenitors to self-renew or undergo malignant transformation43,44 and would explain why OGT-null peripheral T cells fail to clonally expand. However, the effects of OGT on c-Myc are not sufficient to explain all the functions of OGT in T cells. For example, only loss of OGT, but not c-Myc, at the DP stage of thymus development blocks positive selection of mature SP T cells45. In this respect, immunoblot analyses herein reveal the complexity of protein O-GlcNAcylation in T cells indicating that there are many OGT substrates in T cells. Studies in transformed T cells have identified the transcription factors NFκB and NFAT as OGT substrates15,16. The present data reveal the complexity and dynamic nature of the intracellular O-GlcNAcylated T cell proteome and this is likely to be similar to the complexity of protein phosphorylation pathways. The diversity of T cell functions controlled by OGT thus make it probable that the importance of OGT for T cells will be linked to O-GlcNAcylation of multiple targets. In summary, these data highlight the complex roles of protein O-GlcNAcylation for T cell signaling: a previously underappreciated function of T cell nutrient metabolism. The importance of OGT is tightly linked to the metabolically demanding processes of T cell self-renewal and clonal expansion. OGT thus acts as signaling hub to integrate T cell responses to developmental and immune activating stimuli that increase rates of glucose and glutamine transport in T cells.

Online Methods

Mice

All mice were maintained in the University of Dundee in compliance with UK Home Office Animals (Scientific Procedures) Act 1986 guidelines. C57BL/6J mice, *Cd4*-Cre (Tg(Cd4-cre)1Cwi/BfluJ) and *Lck*-Cre (Tg(Lck-cre)548Jxm) were obtained from Jackson laboratories and maintained in-house. The OT-I TCR transgenic mice express a TCR recognizing the ovalbumin (OVA) derived peptide SIINFEKL. *Myc*fl/fl*Cd4*-Cre+ and control *Myc*fl/fl*Cd4*-Cre- were used as previously described46. *GFP-Myc*KI were previously described38. *Ogt*fl (B6.129-Ogttm1Gwh/J) mice, possessing *lox*P restriction sites on either side of the exon encoding amino acids 206-232 of the X-linked *Ogt* gene11, and female

mice bear two copies of the floxed allele while males carry one, were purchased from Jackson Laboratories. Both male and female mice were analyzed, unless otherwise stated in the figure legends. *Pten*^{fl/fl}*Lck*-Cre mice were generated as described previously[33]. When studying normal PTEN-null T cells, to ensure the absence of transformed T cells, experiments were performed using mice between 4 and 6 weeks of age. All mice were on a C57BL/6 genetic background and were used between 6 and 24 weeks old. Wild-type mice used as controls were either WT or WT-Cre[+] or Cre recombinase-negative with various *Pten* or *Ogt* floxed alleles. No randomization was deemed necessary for any animal studies. Analyses of mice phenotypes were performed blinded, and genotypes assigned to the mice after analyses.

Primary T cell cultures

For experiments involving T cell receptor (TCR) stimulation, CD3 antibody (2C11, 5 μg/ml) and CD28 antibody (clone 37.51, eBioscience, 3 μg/ml) were used for polyclonal T cell activation whilst OVA-derived peptides (10 ng/ml unless otherwise stated) were used for OT-I T cell activation for the specified times. peptides OVA peptides used were Q4H7 (SIIQFEHL: Kd 51±9.1 nM), Q4R7 (SIIQFERL: Kd 48±9.5 nM), Q4 (SIIQFEKL: Kd 29±7.2 nM) and N4 (SIINFEKL: Kd 3.7±0.7 nM). Primary T cells were activated to generate CTLs as described previously[19]. To generate T_H1 cells, CD8^{+} T cells were depleted from lymph node preparations using CD8^{+} isolation kits (Miltenyi Biotech or Stemcell Technologies). CD4^{+} cells and APCs were cultured at 1×10^6 cells/ml for 3 days in the presence of CD3 (5 μg/ml) and CD28 (3 μg/ml) antibodies and IL-12 (2 ng/ml, R&D Systems) and IL-2 (20 ng/ml, Proleukin), and then 2 more days in just IL-2 and IL-12. Cells were treated with inhibitors for OGT (OGTi, 4Ac-5S-GlcNAc[22]) or OGA (OGAi, GlcNAcstatin G[23]) as indicated in the figure legends. Inhibitors were produced in-house.

For nutrient starvation experiments, primary T cells were cultured in RPMI 1640 without glucose and glutamine (Biological Industries, USA) supplemented with 10% dialyzed FBS with a 10 kDa cutoff, MEM-amino acids, MEM non-essential amino acids, MEM vitamins, 1 mM sodium pyruvate, Insulin-transferrin-selenium, 50 μM β-mercaptoethanol (all from Thermo Fisher Scientific). Further supplementation was with glucose (Sigma, 10 mM), glutamine (Gibco, 2 mM) or glucosamine (Sigma, 100 μM) unless otherwise indicated in figure legends.

Flow cytometry and cell sorting

For cell surface staining, fluorochrome-conjugated antibodies (BD were used to detect (clone indicated in brackets): CD4 (RM4-5), CD8 (53-6.7), TCRβ (H57-597), B220 (RA3-6B2), CD25 (PC61), CD71 (C2F2), CD98 (RC388), CD44 (IM7), CD62L (MEL-14), CD69 (H1.2F3), (BD Biosciences) CD45.1 (104), CD45.2 (A20), c-kit (2B8), Notch1 (HMN1-12, 1:100), (Biolegend) Notch2 (16F-11), IL-7R (A7R34, 1:100), CD24 (M1/69), and Fc Block (2.4G2) (eBioscience). Antibodies were diluted 1:200 unless otherwise indicated, and 1×10^6 cells were stained in 100 μl. Cells were gated according to their forward scatter and side scatter, and dead cells excluded based on their staining with the LIVE/DEAD fixable dead cell staining kit (Life Technologies).

For intracellular staining for O-GlcNAc, cells were fixed in freshly prepared 1% (vol/vol) paraformaldehyde for 10 min at 37 °C, and then permeabilized in 90% (vol/vol) methanol. After washing, cells were incubated with AlexaFluor 647-conjugated O-GlcNAc antibody (RL2, Novus Biologicals, 1:800) for 20 min at 20-22 °C. For competition based flow, the antibody was pre-incubated with 1 M N-Acetylglucosamine (Sigma Aldrich) prepared in PBS with 1% (vol/vol) FBS for 1 h before adding to the cells and incubating as described. CpOGA treatment (5 μg of enzyme per 1×10^6 cells) was performed for 1 h at 37 °C. Intracellular TCR staining in *ex vivo* thymocytes was done as previously described[47]. Data were acquired on LSR Fortessa or FACSVerse or LSR Canto machines (Becton Dickinson) and analyzed using FlowJo software (TreeStar).

Nutrient uptake measurements

Nutrient uptake was carried out using $0.5–1 \times 10^6$ cells resuspended in 0.4 ml uptake medium. Glucose and glutamine uptake were measured simultaneously in PBS with Ca^{2+} and Mg^{2+} (Life Technologies) containing [^{3}H]-2-deoxyglucose (0.5 μCi/ml), and [^{14}C]-L-Glutamine (0.5 μCi/ml), or individually in glucose-free RPMI (Life Technologies) containing [^{3}H]-2-deoxyglucose (0.5 μCi/ml), and in HBSS with Ca^{2+} and Mg^{2+} (Life Technologies) containing [^{3}H]-L-Glutamine (0.5 μCi/ml). 4 min uptake assays were carried out layered over 0.5 ml of 1:1 silicone oil (Dow Corning 550 (BDH silicone products); specific density, 1.07 g/ml):dibutyl phthalate (Fluka). Cells were pelleted below the oil, following which the aqueous supernatant and the silicon oil/dibutyl phthalate mixture were aspirated, and the cells were washed twice with water. The cell pellet was then lysed in 200 μl NaOH (1 M) and β-radioactivity measured by liquid scintillation counting in a Beckman LS 6500 Multi-Purpose Scintillation Counter (Beckman Coulter).

Quantification of cellular UDP-GlcNAc concentrations

Extraction and downstream processing of nucleotide sugars is based on the previously described method[20]. In brief, 5×10^6 CD8$^+$ T cells and 1×10^6 CD4$^+$ T cells were harvested at different time points after induction, washed with ice-cold PBS, lysed with 70% (vol/vol) ethanol and spiked with 20 pmol of the internal standard GDP-glucose. The samples were lipid-extracted with butanol and the hydrophilic phase was used for nucleotide sugar extraction by graphitized carbon columns (Supelclean™ Envi™-Carb, 3 ml, Supelco). The eluted and freeze dried samples were re-suspended in 40 μl (CD8$^+$) or 20 μl (CD4$^+$) of water and 10 μl (CD8$^+$) or 15 μl (CD4$^+$) were separated by HPLC (Ultimate 3000, Dionex) on a porous graphitic carbon column (HYPERCARB, 30×1 mm, Thermo Scientific™) using a linear gradient of 4–20% (vol/vol) acetonitrile in 0.03% (vol/vol) formic acid (adjusted to pH 9 with ammonia). Nucleotide sugars were detected by electrospray ionisation-tandem mass spectrometry (ESI-MS/MS) using multiple reaction monitoring (MRM) in negative ion mode on a TSQ Quantiva Triple Quadrupole Mass Spectrometer (Thermo Scientific). A standard master mix of nucleotide sugars with known absolute quantities was used as a reference on each day of analysis. In each chromatogram peaks were smoothed and areas integrated (Gaussian) by Xcalibur software. The cellular concentration of UDP-GlcNAc were calculated by using the formula: Quantity of UDP-GlcNAc [pmol] = (sample area UDP-GlcNAc / sample area GDP-Glc) × (standard area GDP Glc / standard area UDP-GlcNAc) × (20 pmol × coefficient UDP-GlcNAc); with "20 pmol"

being the amount of GDP-Glc the sample has been spiked with and the "coefficient UDP-GlcNAc" describing a multiple of GDP-Glc of the actual UDP-GlcNAc concentration in the standard master mix. Accordingly, the amount of UDP-GlcNAc was divided by the number of cells and the total amount of molecules per cell calculated.

Listeria infection

An attenuated Act-A deleted strain of *Listeria monocytogenes* that expresses OVA was used[48]. Wild-type mice were immunized by intravenous injection of 3×10^6 colony forming units. Mice were culled after 3 days and spleens harvested for analysis.

Immunoblotting

TCR stimulated CD8^{+} T cells were purified by magnetic separation (Stemcell Technologies) prior to protein extraction. Standard immunoblotting protocols were used[19]. Blots were probed with antibodies recognizing, dilutions and clone/catalog numbers in brackets: c-Myc (1:1000, #9402), pY694 STAT5 (1:2000, #9351), pan STAT5 (1:1000, #9363), pT389 S6K (1:1000, #9239), S6K (1:1000, #5610) (Cell Signalling Technology), SMC1 (1:5000, A300-055A, Bethyl), β–tubulin (1:5000, H-235) (Santa Cruz), OGT (1:1000, DM17, Sigma) and O-GlcNAc (1:3000, RL2, Abcam). Lysate made from 2×10^8 day 6 CTLs were used for the succinylated wheat germ agglutinin (sWGA) affinity purifications. One half of the lysate was treated with CpOGA and other half was left untreated. Before sWGA affinity purifications, the lysates were precleared with agarose beads for 30 min at 4 °C. 50 μl sWGA beads (L-1020S, Vector Laboratories) were incubated for 16 h with the lysates and beads were washed 4 times with PBS before adding the LDS-loading buffer. For GFP-myc immune-purification, 2×10^8 GFP-Myc[KI] CTLs were lysed and half the lysate was treated with CpOGA or left untreated before the immune-purification. The lysates were incubated with GFP-binder agarose beads (ChromoTek) for 90 min at 4 °C. Beads were washed three times with NP40 buffer before adding the LDS-loading buffer for immunoblotting.

OP9 culture system and assays

OP9 bone marrow stromal cells expressing OP9-DL129 and control OP9 cells were maintained in alpha-MEM supplemented with 50 μM 2-mercaptoethanol, 100 U/ml penicillin, 100 μg/ml streptomycin and 20% (vol/vol) heat-inactivated FBS. Flow-sorted DN3 thymocytes (gated on Thy1^{+}CD44^{-}CD25^{hi}CD4^{-}CD8^{-}) were cultured on OP9 or OP9-DL1 cells for the times indicated in the figure legends. IL-7 was added at 5 ng/ml where indicated. In some experiments total DNs (purified by magnetic depletion of all Lin^{+} cells) were directly used.

Statistical Analyses

Data sets were analyzed using SigmaPlot 12.5 (Systat) or Prism 6.0 (GraphPad). A Shapiro-Wilk test for normality was performed to determine suitable tests for parametric or non-parametric populations. F-tests were performed to determine equal variance of populations, otherwise tests assuming unequal variance were performed. All utilized tests were two-tailed and are stated in the respective figure legends. Multiple comparisons in one-way ANOVA

analyses were corrected for using the Holm-Sidak method. Kaplan-Meier survival analyses were performed for the PTEN$^{fl/fl}$Lck-Cre tumor model.

Supplementary Material

Refer to Web version on PubMed Central for supplementary material.

Acknowledgements

References

1. MacIver NJ, Michalek RD, Rathmell JC. Metabolic regulation of T lymphocytes. Annu Rev Immunol. 2013; 31:259–283. [PubMed: 23298210]

2. Rolf J, et al. AMPKα1: a glucose sensor that controls CD8 T-cell memory. Eur J Immunol. 2013; 43:889–896. [PubMed: 23310952]

3. Sinclair LV, et al. Control of amino-acid transport by antigen receptors coordinates the metabolic reprogramming essential for T cell differentiation. Nat Immunol. 2013; 14:500–508. [PubMed: 23525088]

4. Nakaya M, et al. Inflammatory T cell responses rely on amino acid transporter ASCT2 facilitation of glutamine uptake and mTORC1 kinase activation. Immunity. 2014; 40:692–705. [PubMed: 24792914]

5. Wang R, et al. The Transcription Factor Myc Controls Metabolic Reprogramming upon T Lymphocyte Activation. Immunity. 2011; 35:871–882. [PubMed: 22195744]

6. Hart GW, Housley MP, Slawson C. Cycling of O-linked β-N-acetylglucosamine on nucleocytoplasmic proteins. Nature. 2007; 446:1017–1022. [PubMed: 17460662]

7. Wang Z, et al. Extensive crosstalk between O-GlcNAcylation and phosphorylation regulates cytokinesis. Sci Signal. 2010; 3:ra2. [PubMed: 20068230]

8. Hart GW, Slawson C, Ramirez-Correa G, Lagerlof O. Cross talk between O-GlcNAcylation and phosphorylation: roles in signaling, transcription, and chronic disease. Annu Rev Biochem. 2011; 80:825–858. [PubMed: 21391816]

9. Zhong J, et al. Quantitative phosphoproteomics reveals crosstalk between phosphorylation and O-GlcNAc in the DNA damage response pathway. Proteomics. 2015; 15:591–607. [PubMed: 25263469]

10. Bond MR, Hanover JA. A little sugar goes a long way: the cell biology of O-GlcNAc. J Cell Biol. 2015; 208:869–880. [PubMed: 25825515]

11. Shafi R, et al. The O-GlcNAc transferase gene resides on the X chromosome and is essential for embryonic stem cell viability and mouse ontogeny. Proc Natl Acad Sci USA. 2000; 97:5735–5739. [PubMed: 10801981]

12. O'Donnell N, Zachara NE, Hart GW, Marth JD. Ogt-dependent X-chromosome-linked protein glycosylation is a requisite modification in somatic cell function and embryo viability. Mol Cell Biol. 2004; 24:1680–1690. [PubMed: 14749383]

13. Macintyre AN, et al. The glucose transporter Glut1 is selectively essential for CD4 T cell activation and effector function. Cell Metab. 2014; 20:61–72. [PubMed: 24930970]

14. Kearse KP, Hart GW. Lymphocyte activation induces rapid changes in nuclear and cytoplasmic glycoproteins. Proc Natl Acad Sci USA. 1991; 88:1701–1705. [PubMed: 2000378]

15. Golks A, Tran T-TT, Goetschy JF, Guerini D. Requirement for O-linked N-acetylglucosaminyltransferase in lymphocytes activation. EMBO J. 2007; 26:4368–4379. [PubMed: 17882263]

16. Ramakrishnan P, et al. Activation of the transcriptional function of the NF-κB protein c-Rel by O-GlcNAc glycosylation. Sci Signal. 2013; 6:ra75. [PubMed: 23982206]

17. Carr EL, et al. Glutamine uptake and metabolism are coordinately regulated by ERK/MAPK during T lymphocyte activation. J Immunol. 2010; 185:1037–1044. [PubMed: 20554958]

18. Marko AJ, Miller RA, Kelman A, Frauwirth KA. Induction of Glucose Metabolism in Stimulated T Lymphocytes Is Regulated by Mitogen-Activated Protein Kinase Signaling. PLoS ONE. 2010; 5:e15425. [PubMed: 21085672]

19. Finlay DK, et al. PDK1 regulation of mTOR and hypoxia-inducible factor 1 integrate metabolism and migration of CD8+ T cells. J Exp Med. 2012; 209:2441–2453. [PubMed: 23183047]

20. Turnock DC, Ferguson MAJ. Sugar Nucleotide Pools of Trypanosoma brucei, Trypanosoma cruzi, and Leishmania major. Eukaryotic Cell. 2007; 6:1450–1463. [PubMed: 17557881]

21. Rao FV, et al. Structural insights into the mechanism and inhibition of eukaryotic O-GlcNAc hydrolysis. EMBO J. 2006; 25:1569–1578. [PubMed: 16541109]

22. Gloster TM, et al. Hijacking a biosynthetic pathway yields a glycosyltransferase inhibitor within cells. Nat Chem Biol. 2011; 7:174–181. [PubMed: 21258330]

23. Dorfmueller HC, et al. Cell-Penetrant, Nanomolar O-GlcNAcase Inhibitors Selective against Lysosomal Hexosaminidases. Chemistry & Biology. 2010; 17:1250–1255. [PubMed: 21095575]

24. Ciofani M, Zúñiga-Pflücker JC. Notch promotes survival of pre–T cells at the β-selection checkpoint by regulating cellular metabolism. Nat Immunol. 2005; 6:881–888. [PubMed: 16056227]

25. Ciofani M, et al. Obligatory role for cooperative signaling by pre-TCR and Notch during thymocyte differentiation. J Immunol. 2004; 172:5230–5239. [PubMed: 15100261]

26. Boudil A, et al. IL-7 coordinates proliferation, differentiation and Tcra recombination during thymocyte β-selection. Nat Immunol. 2015; 16:397–405. [PubMed: 25729925]

27. Koch U, Radtke F. Mechanisms of T cell development and transformation. Annu Rev Cell Dev Biol. 2011; 27:539–562. [PubMed: 21740230]

28. Kelly AP, et al. Notch-induced T cell development requires phosphoinositide-dependent kinase 1. EMBO J. 2007; 26:3441–3450. [PubMed: 17599070]

29. Schmitt TM, et al. Induction of T cell development and establishment of T cell competence from embryonic stem cells differentiated in vitro. Nat Immunol. 2004; 5:410–417. [PubMed: 15034575]

30. Wolfer A, Wilson A, Nemir M, Macdonald HR, Radtke F. Inactivation of Notch1 impairs VDJbeta rearrangement and allows pre-TCR-independent survival of early alpha beta Lineage Thymocytes. Immunity. 2002; 16:869–879. [PubMed: 12121668]

31. Balciunaite G, Ceredig R, Fehling HJ, Zúñiga-Pflücker JC, Rolink AG. The role of Notch and IL-7 signaling in early thymocyte proliferation and differentiation. Eur J Immunol. 2005; 35:1292–1300. [PubMed: 15770699]

32. Beverly LJ, Capobianco AJ. Perturbation of Ikaros isoform selection by MLV integration is a cooperative event in Notch(IC)-induced T cell leukemogenesis. Cancer Cell. 2003; 3:551–564. [PubMed: 12842084]

33. Hagenbeek TJ, et al. The loss of PTEN allows TCR alphabeta lineage thymocytes to bypass IL-7 and Pre-TCR-mediated signaling. J Exp Med. 2004; 200:883–894. [PubMed: 15452180]

34. Suzuki A, et al. T cell-specific loss of Pten leads to defects in central and peripheral tolerance. Immunity. 2001; 14:523–534. [PubMed: 11371355]

35. Hagenbeek TJ, Spits H. T-cell lymphomas in T-cell-specific Pten-deficient mice originate in the thymus. Leukemia. 2008; 22:608–619. [PubMed: 18046443]

36. Liao W, Lin J-X, Leonard WJ. Interleukin-2 at the crossroads of effector responses, tolerance, and immunotherapy. Immunity. 2013; 38:13–25. [PubMed: 23352221]

37. Preston GC, et al. Single cell tuning of Myc expression by antigen receptor signal strength and interleukin-2 in T lymphocytes. EMBO J. 2015; 34:2008–2024. [PubMed: 26136212]

38. Huang C-Y, Bredemeyer AL, Walker LM, Bassing CH, Sleckman BP. Dynamic regulation of c-Myc proto-oncogene expression during lymphocyte development revealed by a GFP-c-Myc knock-in mouse. Eur J Immunol. 2008; 38:342–349. [PubMed: 18196519]

39. Chou TY, Hart GW, Dang CV. c-Myc is glycosylated at threonine 58, a known phosphorylation site and a mutational hot spot in lymphomas. J Biol Chem. 1995; 270:18961–18965. [PubMed: 7642555]

40. Doedens AL, et al. Hypoxia-inducible factors enhance the effector responses of CD8(+) T cells to persistent antigen. Nat Immunol. 2013; 14:1173–1182. [PubMed: 24076634]

41. Ho P-C, et al. Phosphoenolpyruvate Is a Metabolic Checkpoint of Anti-tumor T Cell Responses. Cell. 2015; 162:1217–1228. [PubMed: 26321681]

42. Chang C-H, et al. Metabolic Competition in the Tumor Microenvironment Is a Driver of Cancer Progression. Cell. 2015; 162:1229–1241. [PubMed: 26321679]

43. Dose M, et al. c-Myc mediates pre-TCR-induced proliferation but not developmental progression. Blood. 2006; 108:2669–2677. [PubMed: 16788099]

44. Zhang J, et al. Differential Requirements for c-Myc in Chronic Hematopoietic Hyperplasia and Acute Hematopoietic Malignancies in Pten-null Mice. Leukemia. 2011; 25:1857–1868. [PubMed: 21926961]

45. Dose M, et al. Intrathymic proliferation wave essential for Vα14$^+$ natural killer T cell development depends on c-Myc. Proc Natl Acad Sci USA. 2009; 106:8641–8646. [PubMed: 19423665]

46. Mycko MP, et al. Selective requirement for c-Myc at an early stage of V(alpha)14i NKT cell development. J Immunol. 2009; 182:4641–4648. [PubMed: 19342639]

47. Hinton HJ, Clarke RG, Cantrell DA. Antigen receptor regulation of phosphoinositide-dependent kinase 1 pathways during thymocyte development. FEBS Lett. 2006; 580:5845–5850. [PubMed: 17027005]

48. Pearce EL, Shen H. Generation of CD8 T cell memory is regulated by IL-12. J Immunol. 2007; 179:2074–2081. [PubMed: 17675465]
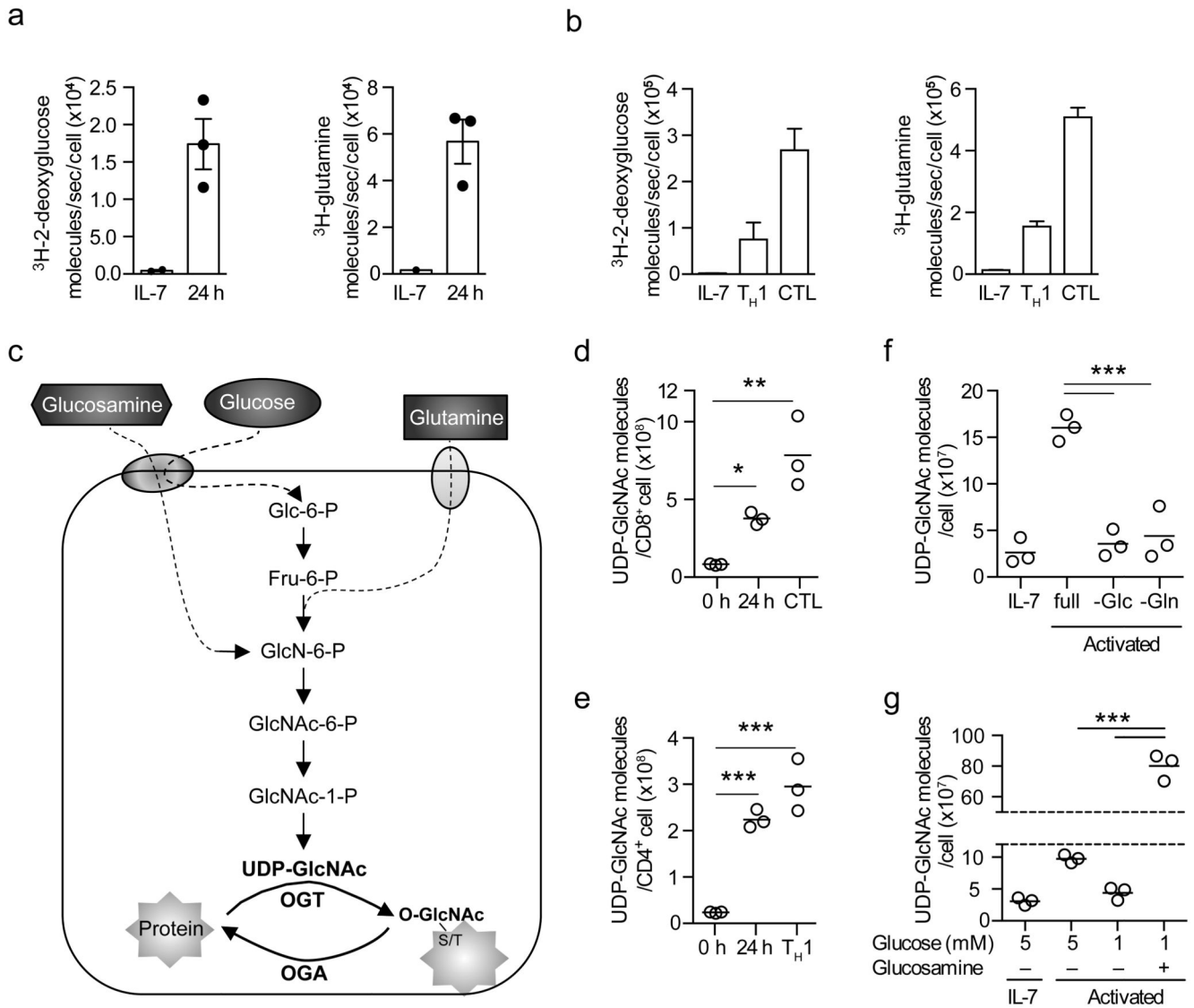
Figure 1.
T cells utilize glucose and glutamine intake for UDP-GlcNAc biosynthesis through a key nutrient-sensing pathway. (**a**) Uptake of ^{3}H-2-deoxyglucose or ^{3}H-glutamine by naïve lymph node (LN) T cells maintained in IL-7 (IL-7) (n=2 mice) or TCR stimulated with CD3/CD28 antibodies for 24 hours (n=3 mice). (**b**) Uptake of ^{3}H-2-deoxyglucose or ^{3}H-glutamine by effector CD8$^+$ T cells (CTL) or CD4$^+$ T helper cells (T$_H$1) or naïve T cells maintained in IL-7 for 24 hours (IL-7). (**c**) Glucose and glutamine intake feed into the hexosamine biosynthesis pathway that produces UDP-N-Acetylglucosamine (UDP-GlcNAc), which is the substrate for OGT. Glucosamine bypasses the rate-limiting step of synthesis of glucosamine-6-phosphate, and the requirement for glucose and glutamine to make UDP-GlcNAc. (**d-g**) UDP-GlcNAc concentrations measured by LC-MS/MS (n=3 mice each). (**d**) UDP-GlcNAc in naïve (0 h) CD8$^+$ T cells, CD3/CD28 stimulated CD8$^+$ T cells (24 h) and CTLs. (**e**) UDP-GlcNAc in naïve (0 h) CD4$^+$ T cells, CD3/CD28 stimulated CD4$^+$ T cells

(24 h) and T_H1 effectors. (**f**) UDP-GlcNAc concentrations in OT-I T cells either unstimulated (maintained in IL-7, IL-7) or activated for 24 hours with peptide in full medium or medium lacking either glucose (-Glc) or glutamine (-Gln). (**g**) UDP-GlcNAc concentrations in OT-I cells stimulated in medium supplemented as indicated. *$P < 0.05$, ** $P < 0.01$, *** $P < 0.001$ (one-way ANOVA, n=3 mice each). Data are from one experiment representative of 3 (**a,** mean and s.e.m. of biological replicates), 4 (**b**, mean and s.e.m. of technical replicates, n=1), and one experiment each (**d-g**).
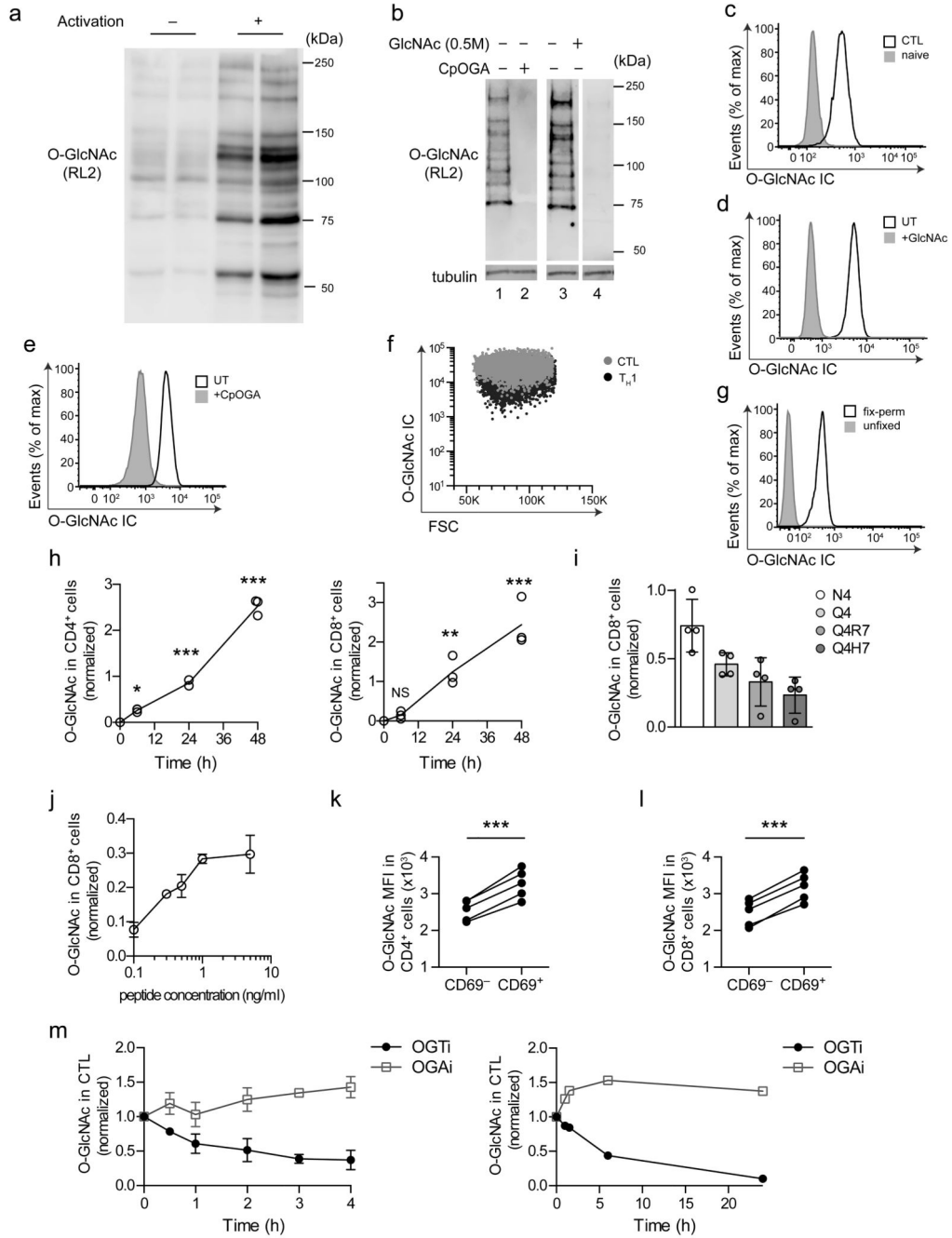
Figure 2.
TCR activation upregulates O-GlcNAcylation in T cells. (**a**) Immunoblot analysis of O-GlcNAc in naïve (–) and 24 hours CD3/CD28-activated (+) T cells (n=2 mice). (**b**) Immunoblotting of CTLs lysates either untreated (lanes 1,3,4) or treated with CpOGA (lane 2). Immunoblotting was with the O-GlcNAc antibody (lanes 1,2), or the antibody was pre-incubated with 0.5 M N-Acetylglucosamine (GlcNAc) (lanes 3,4). (**c**) Intracellular flow cytometric analysis with an O-GlcNAc antibody (RL2) of CTLs and naïve CD8^{+} T cells. (**d**) Flow cytometric analysis of naïve CD8^{+} T cells with the O-GlcNAc antibody that was either

pre-incubated with free N-Acetylglucosamine (+GlcNAc) or not. (**e**) O-GlcNAc flow cytometric analysis of CTLs treated with CpOGA. (**f**) Dot plot showing forward scatter (FSC) and O-GlcNAc intensities of cells derived from CTLs (grey) and T_H1 (black) cultures (n=1 mouse). Pearson's correlation=-0.072 (CTL), 0.036 (T_H1). (**g**) 6 hour activated OT-I T cells were either fixed, permeabilized and analyzed, or live cells were analyzed for O-GlcNAc flow cytometry. (**h**) Naïve LN T cells (n=3 mice) were stimulated with CD3/CD28 antibodies for 6, 24 or 48 hours, and their O-GlcNAc mean fluorescence intensities (MFI) were normalized as a fractional difference to naïve resting T cells (gated on CD62L^{hi}, CD44^{lo}). (**i**) O-GlcNAc flow cytometry data normalized as in (h) of OT-I CD8$^+$ T cells stimulated for 24 hours with OVA-derived peptides. O-GlcNAc MFI of total CD8$^+$ T cells was normalized to the MFI of unactivated cells (n=4 mice, pooled from 2 experiments). (**j**) O-GlcNAc MFI (normalized to naïve cells) of OT-I T cells stimulated with serial dilutions of Q4 peptide for 6 hours (n=3 mice). (**k-l**) O-GlcNAc flow cytometric analysis in CD69$^+$ or CD69$^-$ splenic CD4$^+$ (**k**) and CD8$^+$ (**l**) T cells isolated from mice (n=5) infected i.v. with *Listeria.* (**m**) Normalized (to untreated) O-GlcNAc MFI in CTLs treated for the indicated times with an OGA inhibitor (OGAi) or an OGT inhibitor (OGTi). *$P < 0.05$, **$P < 0.01$, ***$P < 0.001$ (**h**, One-way ANOVA, compared to 0 h time point, **k,l,** paired t-test). Data are representative of 2 similar experiments (**a**) 1 experiment (**b**), 3 experiments (**h,i,j,** mean ±s.d. shown), experiments shown in **c-g** are representative of at least 5 experiments, (**m**) left, mean (±s.d.) of n=5 cultures from 2 experiments shown, right, n=1, representative of 2 experiments.
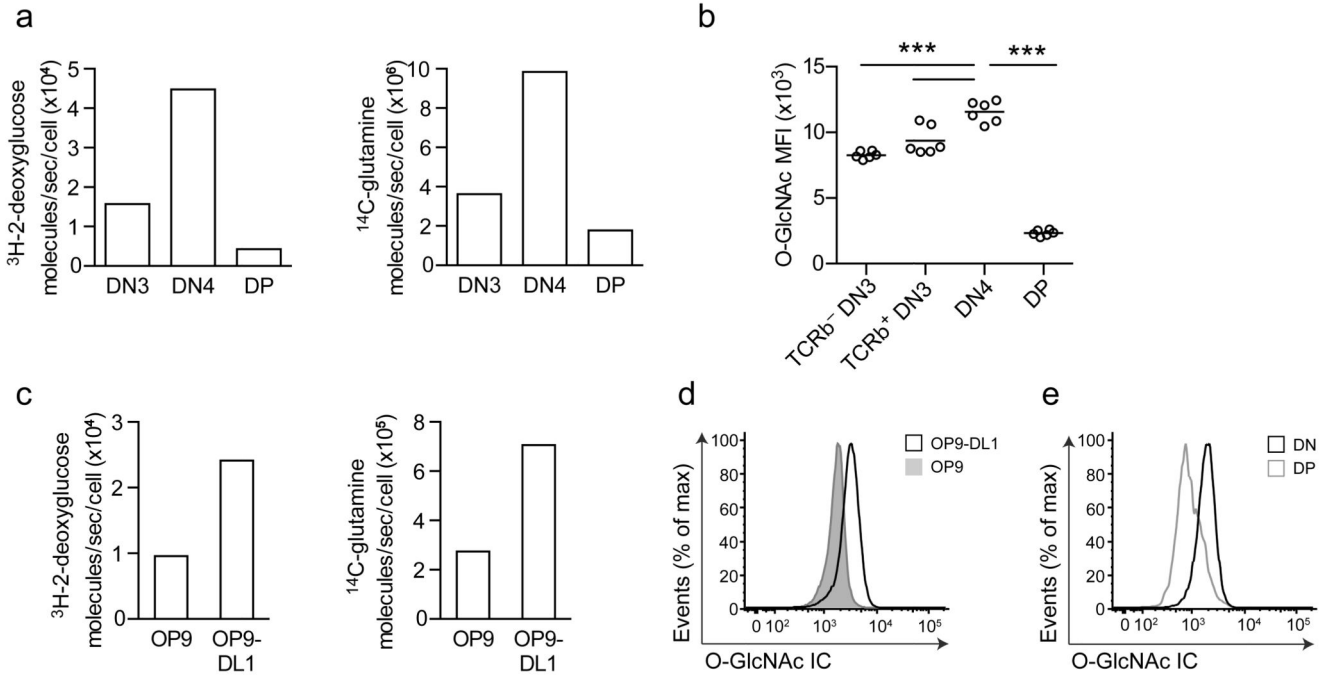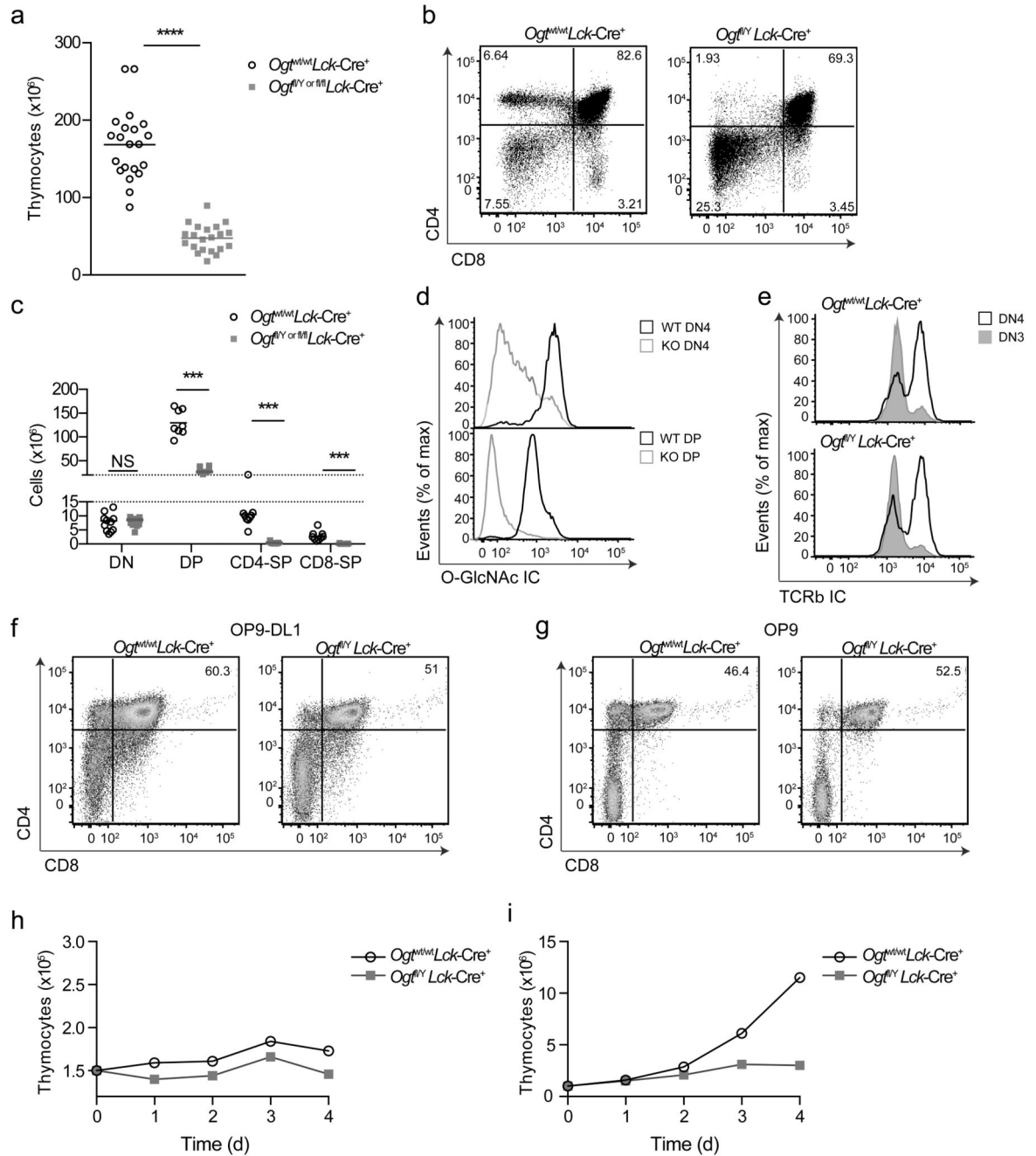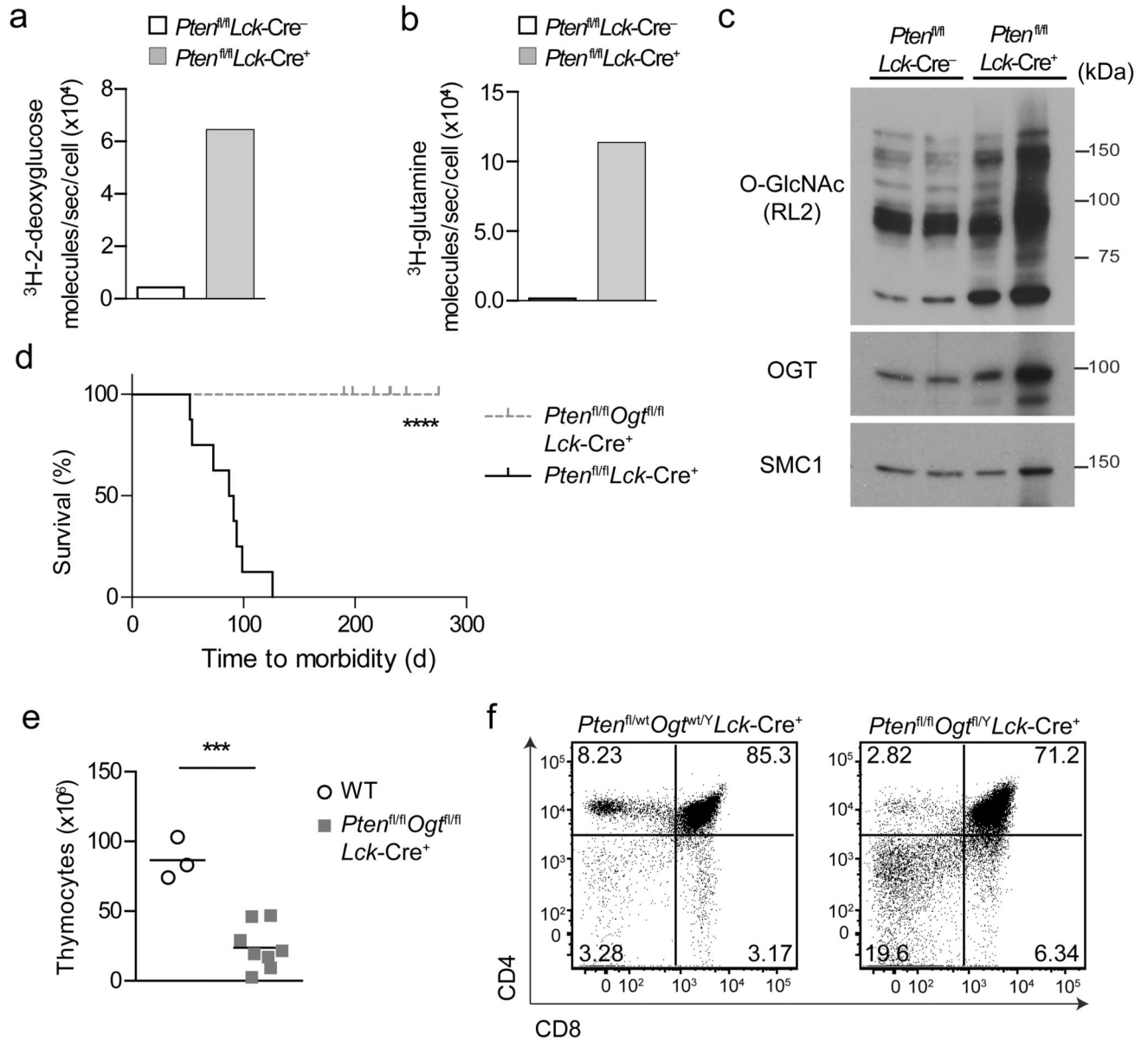
Figure 3.

Glucose and glutamine uptake are regulated during thymocyte β-selection and feed into O-GlcNAcylation. (**a**) Uptake of ^{3}H-2-deoxyglucose and ^{14}C-glutamine in thymocytes pooled from 10 wild-type mice sorted into DN3, DN4 and DP subsets. (**b**) Intracellular flow cytometric analysis of O-GlcNAc and TCRβ was done along with surface markers for the different subsets (n=6 mice). (**c**) DN3-4 thymocytes were cultured on OP9 or OP9-DL1 in the presence of IL-7 (5 ng/ml) for 2 days. Uptake of ^{3}H-2-deoxyglucose and ^{14}C-glutamine was measured, as well as (**d**) intracellular O-GlcNAc levels in either total Thy1$^+$ cells on OP9 or OP9-DL1, or (**e**) cells grown on OP9-DL1 and gated on DP (CD4$^+$CD8$^+$) and DN (CD4$^-$CD8$^-$) thymocytes. ***$P < 0.001$ (One-way ANOVA). Data are from 1 experiment (**a**), 2 pooled experiments and representative of 5 similar experiments (**b**), 1 experiment representative of 3 independent experiments (**c,d**).

Figure 4.
Loss of OGT at the DN stage of T cell development leads to a strong block in T cell development. (**a**) Total numbers of cells isolated from thymi of $Ogt^{wt/wt}Lck$-Cre$^+$ mice (n=21) and $Ogt^{fl/Y\ or\ fl/fl}Lck$-Cre$^+$ mice (n=21) are plotted. (**b**) Representative flow cytometry of CD4 and CD8 expression on Thy1$^+$ thymocytes from $Ogt^{wt}Lck$-Cre$^+$ and $Ogt^{fl/Y}Lck$-Cre$^+$ mice from (**a**). (**c**) Quantification of thymic subsets in 6- to 12-week old $Ogt^{wt/wt}Lck$-Cre$^+$ (n=9) and $Ogt^{fl/Y\ or\ fl/fl}Lck$-Cre$^+$ mice (n=9). (**d**) Flow cytometric histogram plots showing intracellular O-GlcNAc levels in $Ogt^{wt/wt}Lck$-Cre$^+$ (WT) and

$Ogt^{fl/Y}Lck$-Cre$^+$ (KO) DN4 and DP subsets. (**e**) Intracellular flow cytometry for TCRβ (pre-TCR) in DN3 and DN4 subsets from $Ogt^{wt/wt}Lck$-Cre$^+$ and $Ogt^{fl/Y}Lck$-Cre$^+$ thymi. (**f-i**) OGT$^{wt/wt}$Lck-Cre$^+$ and $Ogt^{fl/Y}Lck$-Cre$^+$ DN thymocytes were cultured for 6 days on OP9 or OP9-DL1 feeder cells, in the presence or absence of 5 ng/ml IL-7. 3 days after culture on OP9-DL1 (**f**) or OP9 (**g**), $Ogt^{wt/wt}Lck$-Cre$^+$ and $Ogt^{fl/Y}Lck$-Cre$^+$ thymocytes were stained for CD4 and CD8. (**h,i**) Proliferation of $Ogt^{wt/wt}Lck$-Cre$^+$ and $Ogt^{fl/Y}Lck$-Cre$^+$ DN thymocytes cultured on OP9-DL1 feeders (**h**) or OP9 (**i**) in the presence of 5 ng/ml IL-7. NS, not significant (P=0.251), ***$P < 0.001$, ****$P < 0.0001$ (unpaired t-test (**a**), Mann-Whitney Rank Sum test (**c**)). Data are cumulative (**a,c**) or representative of >40 mice (**b**), 3 mice (**d**), 3 mice (**e**) and (**f-i**) are representative of 3 independent experiments.

Figure 5.
Loss of OGT prevents transformation of PTEN-null thymocytes. Analysis of (**a**) ^{3}H-2-deoxyglucose uptake and (**b**) ^{3}H-glutamine uptake in cells isolated from thymi of *Pten*$^{fl/fl}$*Lck*-Cre$^-$ and from thymic tumors of *Pten*$^{fl/fl}$*Lck*-Cre$^+$ mice (n=1). (**c**) Immunoblot analysis of global O-GlcNAcylation and OGT in equal numbers of thymic lymphoma cells from two representative *Pten*$^{fl/fl}$*Lck*-Cre$^+$ mice and total thymocytes from two *Pten*$^{fl/fl}$*Lck*-Cre$^-$ mice. SMC1 was used as loading control. (**d**) Kaplan-Meier survival plot comparing kinetics of tumor development in *Pten*$^{fl/fl}$*Lck*-Cre$^+$ (n=8) mice compared with *Pten*$^{fl/fl}$*Ogt*$^{fl/fl \text{ or } fl/Y}$*Lck*-Cre$^+$ (n=10) mice. (**e**) Average thymocytes numbers in old *Pten*$^{fl/fl}$*Ogt*$^{fl/fl \text{ or } fl/Y}$*Lck*-Cre$^+$ mice (n=8, average age=239 days), as compared to wild-type (WT) mice of similar age (n=3). (**f**) Representative flow cytometric plots of CD4 and CD8

expression in Thy1$^+$ thymocytes derived from *Pten*$^{fl/wt}$*Ogt*^{wt}*Lck*-Cre$^+$ and *Pten*$^{fl/fl}$*Ogt*$^{fl/Y}$*Lck*-Cre$^+$ thymi at 6 weeks of age. ***P = 0.000228, ****P < 0.0001 (Log rank (Mantel-Cox) test (**d**), unpaired t-test (**e**)). Data are from one experiment, representative of 3 (**a-c**), cumulative (**d,e**), and representative of 3 mice (**f**).
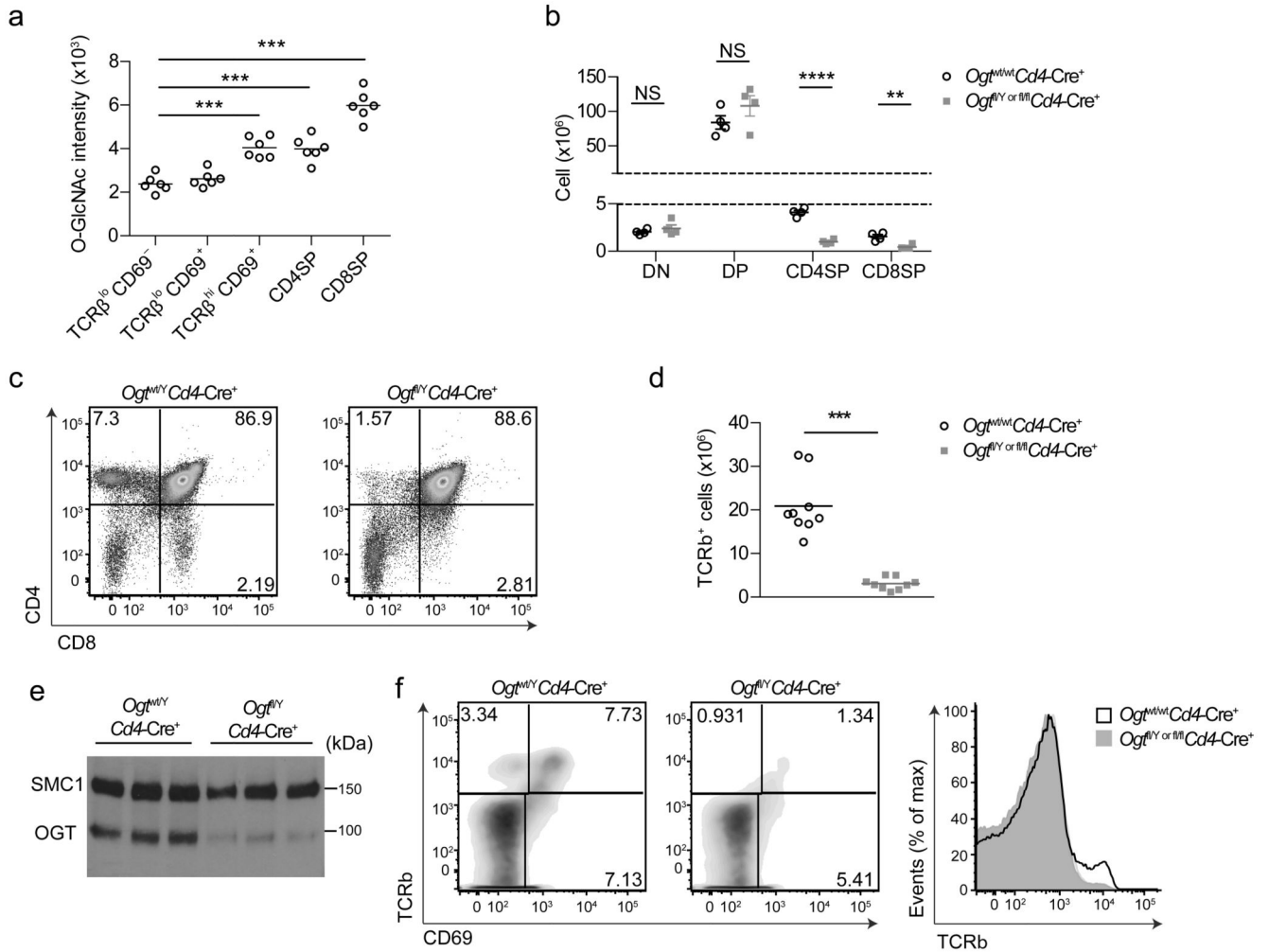
Figure 6.
Deletion of OGT at the DP stage of T cell development blocks positive selection. (**a**) O-GlcNAc flow cytometric analyses in quiescent DPs (TCRβ^{lo}CD69$^-$), pre-selected (TCRβ^{lo}CD69^{hi}), post-selected (TCRβ^{hi}CD69^{hi}) thymocytes, and mature CD4SP and CD8SP (TCRβ^{hi}CD69^{lo}CD24^{lo}). Populations were electronically gated as depicted in Supplementary Fig. 2a. (**b**) Quantification of thymic subsets cell numbers in 6- to 12-week old $Ogt^{wt/wt}Cd4$-Cre$^+$ (n=4) and $Ogt^{fl/fl}Cd4$-Cre$^+$ mice (n=4). (**c**) Representative flow cytometry plots of CD4 and CD8 expression on Thy1$^+$ thymocytes from $Ogt^{wt/Y}Cd4$-Cre$^+$ and $Ogt^{fl/Y}Cd4$-Cre$^+$ mice. (**d**) Total numbers of TCRβ$^+$ cells isolated from $Ogt^{wt/wt}Cd4$-Cre$^+$ spleens (n=9) and $Ogt^{fl/fl}Cd4$-Cre$^+$ spleens (n=9) are plotted. (**e**) Immunoblotting analysis of OGT and loading control SMC1 for thymocytes from 3 $Ogt^{wt/Y}Cd4$-Cre$^+$ and 3 $Ogt^{fl/Y}Cd4$-Cre$^+$ mice. (**f**) Representative flow cytometry for TCRβ expression and CD69 expression in WT and KO thymocytes (gated on Thy1$^+$ living cells). To the right, histogram of TCRβ expression is shown in $Ogt^{wt/Y}Cd4$-Cre$^+$ (n=1) and $Ogt^{fl/Y}Cd4$-Cre$^+$ (n=3) thymocytes. NS, not significant, ** P=0.00437, ***$P< 0.001$, **** $P< 0.0001$ (One-way ANOVA (**a**), t- tests (**b,** mean ± s.e.m), Mann-Whitney Rank Sum test (**d**)). Data are cumulative (**a,b,d**), representative of 9 mice (**c,f**), and one experiment (**e**).
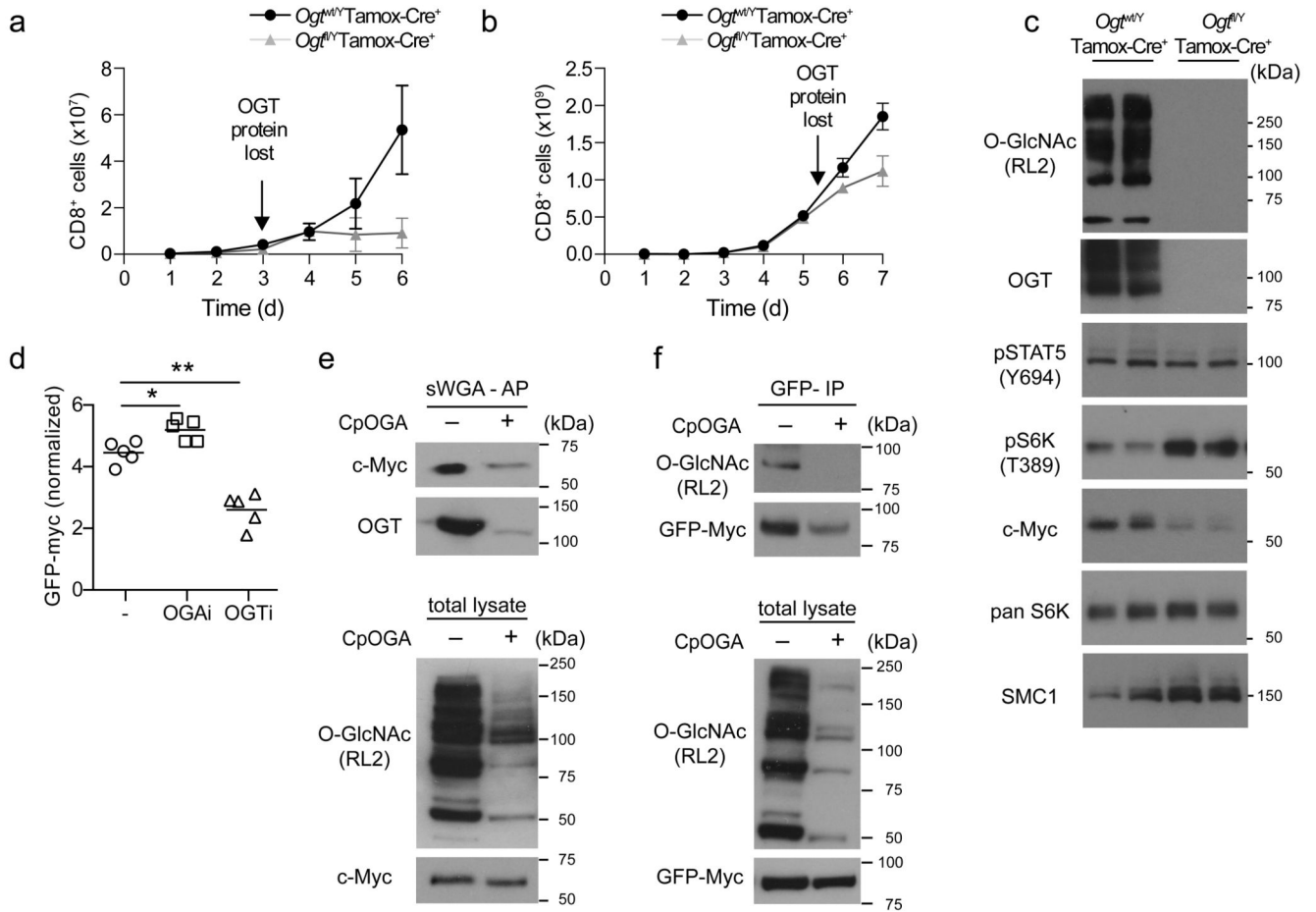
Figure 7.
Protein O-GlcNAcylation regulates c-Myc expression and T cell clonal expansion. (**a,b**) Total numbers of cells obtained on each day of primary CTLs cultures of splenic T cells from *Ogt*wtTamox-Cre+ or *Ogt*fl/YTamox-Cre+ mice. In (**a**), naïve splenocytes were treated with 4-OHT for 4 hours prior to washing out and activation. In (**b**) 4-OHT treatment was done on day 5. (**c**) Cells cultured as in (**b**) were immunoblotted as indicated. (**d**) GFP-MycKI LN T cells (n=5 mice) were stimulated for 6 hours with CD3/CD28 antibodies in the presence of an OGA or an OGT inhibitor (OGAi, OGTi). GFP-myc MFI normalized to naïve T cells is plotted. (**e**) sWGA affinity purification (AP) from OT-I CTLs lysates were analyzed by immunoblotting for c-Myc. The cell lysate were either left untreated or treated with CpOGA before the affinity purification and immunoblotting for c-Myc and OGT. Total lysates were probed for total protein O-GlcNAcylation and c-Myc. (**f**) GFP immune-purification (IP) was done from GFP-MycKI CTLs lysate that were either left untreated or CpOGA treated. Immune-purified GFP-Myc was probed with RL2 antibody. The lysates were immunoblotted for total protein O-GlcNAcylation and c-Myc. *P= 0.017, ** $P<$ 0.001 (one-way ANOVA). Data are from one experiment each (**a,b**, mean ± s.d. n=3 mice for each genotype) and representative of 2 (**a**) and 5 (**b**) experiments, data are from 2 pooled experiments (**d**), and data in (**c,e,f**) are from one experiment and representative of 2 (**c**), 2 (**e**) and 4 (**f**) experiments.
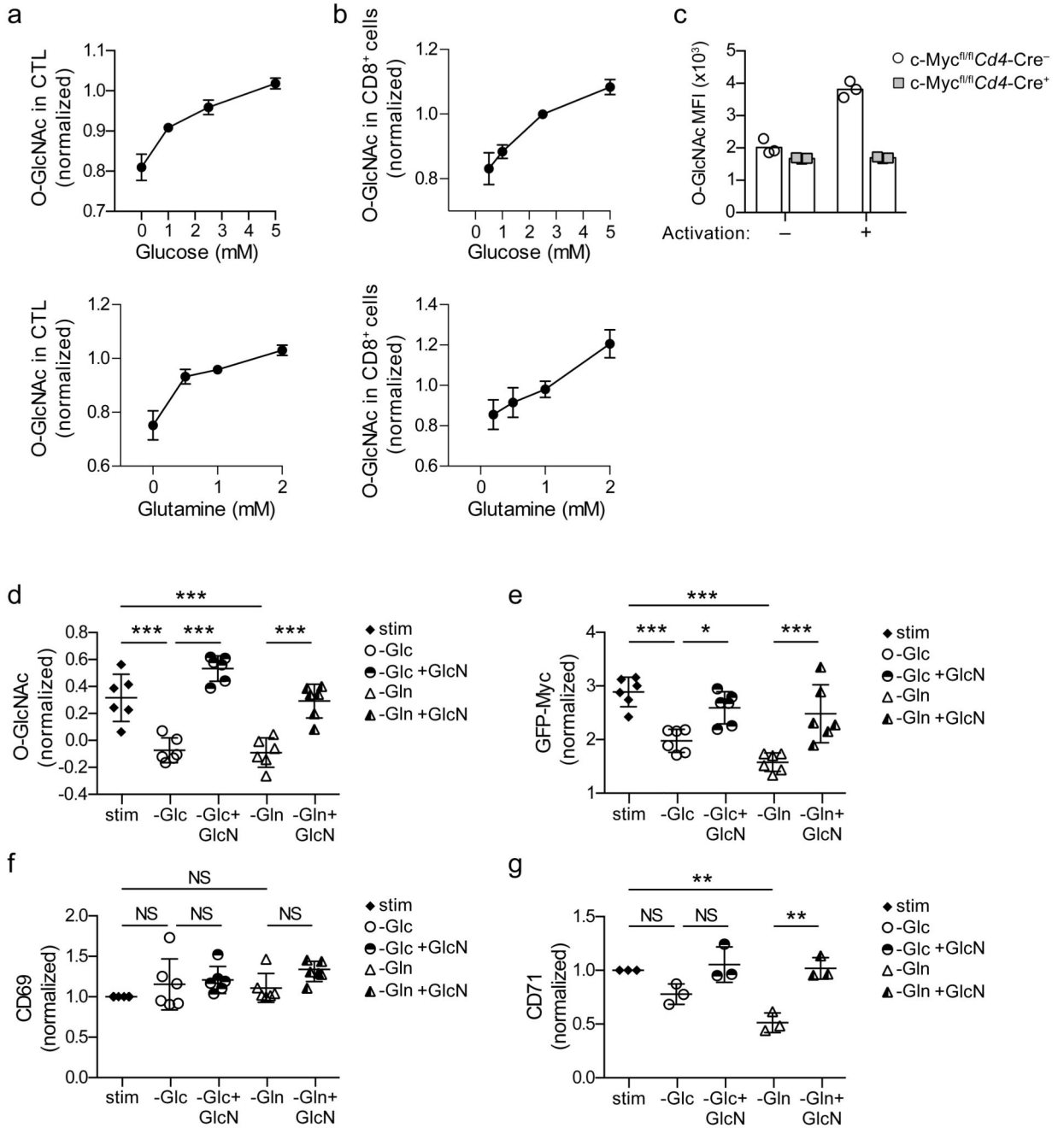
Figure 8.
c-Myc regulates protein O-GlcNAcylation through glucose and glutamine flux. (**a**) O-GlcNAc flow cytometric analyses in day 7 CTLs (n=6 mice) cultured for 20 hours in RPMI containing different doses of glucose or glutamine in the medium. O-GlcNAc MFI was normalized to the MFI of CTLs grown in the highest concentration of glucose or glutamine. (**b**) O-GlcNAc flow cytometric analyses in 6 hours activated OT-I T cells (n=3 mice) cultured in RPMI containing different doses of glucose or glutamine in the medium, normalized as in (**a**). (**c**) O-GlcNAc flow cytometric analysis in total live CD8+ T cells from

LN of *Myc*^{fl/fl}*Cd4*-Cre⁻ (n=3) and *Myc*^{fl/fl}*Cd4*-Cre⁺ (n=3) mice, stimulated with CD3/CD28 antibodies for 18 hours (+), or fixed directly post-isolation (–). (**d-g**) GFP-myc^{KI} LN T cells (n=6 mice) were activated for 6–24 hours in either complete medium, or in medium lacking glucose (-Glc) supplemented or not with glucosamine (+GlcN), or lacking glutamine (-Gln) supplemented or not with glucosamine (+GlcN). (**d**) O-GlcNAc MFI measured by intracellular flow cytometry after 6 hours and normalized (n=6) to unstimulated cells. (**e**) GFP-myc fluorescence intensity measured after 6 hours and normalized to unstimulated cells. (**f**) CD69 MFI measured after 6 hours, and (**g**) CD71 MFI (n=3 mice) measured after 24 hours, were normalized to cells stimulated in full medium. NS, not significant, *$P < 0.05$, **$P < 0.01$, ***$P < 0.001$ (one-way ANOVA). Data are pooled from 2 experiments (**a,** mean ± s.e.m of n=6 (glucose) n=5 (glutamine)) and representative of 2 experiments (**a**) or one experiment (**b,** mean ± s.d. of n=3), one experiment (**c**) or pooled from 2 experiments (**d-g,** mean ± s.d.).